Structure of the A20 OTU domain and mechanistic insights into deubiquitination

David Komander, David Barford

Structure of the A20 OTU domain and mechanistic insights into deubiquitination

David Komander[#] and David Barford

Section of Structural Biology, The Institute of Cancer Research, Chester Beatty Laboratories, 237 Fulham Road, London SW3 6JB, UK.

Corresponding author, email: david.komander@icr.ac.uk, phone: +44 20 7153 5447, fax: +44 20 7153 5457

Running title: A20 OTU domain structure

Word count: 5100

Key words: Lys63-linked ubiquitin, cytokine signalling, NF-κB, IKK, TAK1, TRAF, ABIN, deubiquitinating enzyme

Abstract

The NF-κB regulator A20 antagonises IKK activation by modulating Lys63-linked polyubiquitination of cytokine receptor associated factors including TRAF2/6 and RIP1. Here we describe the crystal structure of the N-terminal Ovarian Tumour (OTU) deubiquitinase domain of A20, which differs from other deubiquitinases but shares the minimal catalytic core with Otubain-2. Analysis of conserved surface regions allows prediction of ubiquitin binding sites for the proximal and distal ubiquitin molecules. Structural and biochemical analysis suggests a novel architecture of the catalytic triad, which might be present in a subset of OTU domains including Cezanne and TRABID. Biochemical analysis shows a preference of the isolated A20 OTU domain for Lys48-linked tetraubiquitin *in vitro* suggesting that additional specificity factors might be required for the physiological function of A20 in cells.

(127 words)

Introduction

Tumour necrosis factor α (TNFα) and cytokines such as interleukin-1 activate inflammatory signalling cascades leading to the stimulation of transcription factors such as nuclear factor κB (NF-κB) (reviewed in [1, 2]). Amongst the TNFα induced genes is A20 [3], a negative regulator of NF-κB, which establishes a negative feedback loop to terminate the response (reviewed in [4, 5]). Mice lacking A20 develop severe inflammation and are hyper-responsive to TNFα and lipopolysaccharide, due to the failure to repress TNFα induced NF-κB signalling [6, 7]. Elegant work by Wertz *et al.* [8] has illuminated the mechanism of A20 action through dual ubiquitin editing functions (reviewed in [5]).

Ubiquitination has been established as a key signalling event at multiple levels of NF-κB activation (reviewed in [9-12]). Immediately in response to cytokine stimulation, polyubiquitin chains linked through Lys63 are assembled on receptor interacting proteins (RIP) including RIP1, TNFα receptor interacting protein-2 (TRAF2), TRAF6, and NF-κB essential modifier (NEMO) [9]. Such K63-linked ubiquitin chains act as scaffolds for the TGFβ activated kinase-1 (TAK1) and Inhibitor of κB (IκB) kinase (IKK) protein kinase complexes, which incorporate subunits with specific ubiquitin binding domains (NEMO in the IKK complex, and TAB2 or TAB3 in the TAK1 complex) [9]. Co-localisation enables TAK1 autophosphorylation of its activation segment, and subsequently TAK1 phosphorylates and activates downstream kinases including IKKβ. IKKβ then phosphorylates the cytoplasmic inhibitor of κB (IκB):NF-κB complex, which triggers Lys48-linked polyubiquitination and proteasomal degradation of IκB, releasing NF-κB to enter the nucleus and activate transcription of target genes (reviewed in [1, 2]). A20 acts as a negative regulator by interfering with NF-κB signalling pathways at the level of TRAF and RIP1 ubiquitination by disassembling Lys63-linked polyubiquitin chains from TRAF2/6 and RIP1, and subsequently replacing them with Lys48-linked polyubiquitin [7, 8]. This dual action not only antagonises downstream signalling, but also targets the substrates for proteasomal degradation [5].

A20 is a 790 amino acid protein with an N-terminal Ovarian Tumour (OTU) domain (residues 1-370) and seven repeats of A20-like zinc fingers (ZnF) domains [8]. The ZnF domains confer E3 ubiquitin ligase activity, and bind to UbcH5-family E2 ubiquitin conjugating enzymes to generate Lys48-linked polyubiquitin chains [8, 13]. Recently, A20-like ZnF domains have also been shown to possess ubiquitin binding capacity [13, 14]. In addition, the ZnF domains are involved in A20 oligomerisation [15], and protein-protein interactions with ABIN (A20-binding inhibitor of NF-κB) family members [5, 16] and TAX1 binding protein-1 [17]. The N-terminal OTU domain of A20 is a deubiquitinase [8, 18]. OTU domains share a Cys protease catalytic triad common to other deubiquitinase families, and A20 has been shown to hydrolyse Lys48-, Lys63- and branched ubiquitin chains *in vitro* and *in vivo* [18, 19]. Structurally, OTU domains belong to a relatively uncharacterised class of deubiquitinating enzymes. The structure of Otubain-2, a OTU domain protein with 224 amino acids, has been reported, but sequence identity to A20 is low (15 % identical) (pdb-id 1tff, [20]). Otubain-2 is structurally divergent from other Cys-dependent deubiquitinases such as ubiquitin specific protease (USP) or ubiquitin C-terminal hydrolase (UCH) domains [20].

Here, we analyse the A20 OTU domain crystal structure, and provide biochemical insight into the catalytic mechanism, and *in vitro* activity.

Material and Methods

Cloning

Full-length A20 was cloned from human cDNA, and shorter constructs were PCR amplified using standard methods. The A20 OTU domain (residues 1-366) ($A20^{1-366}$) was cloned into the pGEX6P1 vector (GE Healthcare, N-terminal GST-tag with Prescission cleavage site) using *BamH*I and *Not*I. The pOPIN-E (C-terminal His_6 tag) construct was prepared with the Infusion 2.0 system (Clontech). Mutagenesis was performed using the Quikchange site directed mutagenesis kit (Stratagene). All constructs were verified by sequencing.

Protein purification and crystallisation

GST-tagged $A20^{1-366}$ was expressed in *E.coli* BL21 (DE3) cells, at 25 °C for 16 hrs after induction with 200 μM IPTG at an OD_{600} of 0.8. Cells from 2 l culture were lysed by sonication in 50 ml lysis buffer (270 mM sucrose, 50 mM Tris [pH 8.0], 1 mM EDTA, 1 mM EGTA, 10 mM sodium β-glycerophosphate, 50 mM sodium fluoride, 10 mM β-mercaptoethanol, 1 mM benzamidine, 0.1 mg/ml DNAseI 1 mg/ml lysozyme), and cleared by centrifugation. The cleared lysate was incubated with 6 ml equilibrated glutathione-S-sepharose 4B resin (GE Healthcare) for 1 hr, and subsequently washed with 50 ml lysis buffer, 500 ml buffer A (25 mM Tris [pH 8.5], 1 mM EDTA, 5 mM DTT) plus 500 mM NaCl, and 500 ml buffer A plus 200 mM NaCl. The GST-tag was cleaved on the resin with 200 μg GST-tagged PreScission protease overnight. The cleaved A20 OTU domain was subjected to anion exchange chromatography (HiTrap Q FF) where it eluted as a single peak in a NaCl gradient from 50 to 500 mM. The peak fractions were concentrated to 5 ml and subjected to gel filtration (Superdex75) in buffer A with 200 mM NaCl. The protein was concentrated to 13 mg/ml using a VivaSpin (10 kDa MW cut-off) concentrator and used in crystallisation. For structure determination by anomalous phasing techniques, the protein was produced in the *E. coli* B834 strain and grown in minimal medium with seleno-methionine substituting for Met, using standard protocols, and purified with

increased DTT concentration (10 mM) in all buffers. All protein purifications were performed at 4°C.

The A20 OTU domain structure was determined from crystals grown from 1.3-1.6 M magnesium sulphate, 0.1 M MES [pH 6.5-6.9] after 7 days at 14°C. For synchrotron data collection, crystals were soaked in mother liquor containing 15 % ethylene glycol, and frozen in a nitrogen cryostream.

Data collection, phasing and refinement

Diffraction data on A20 OTU domain crystals were collected at the ESRF, beamlines ID29 and ID14-2. A three wavelength MAD dataset was collected to 3.7 Å resolution from SeMet crystals and used for phasing. An initial set of sites was determined with the SHELX/hkl2map [21] suite, and site refinement was performed in SHARP [22], resulting in phases to 3.7 Å (Table I). SHARP determined a solvent content of 62.8 %, resulting in a Matthews coefficient of 3.4 with four A20 molecules in the asymmetric unit. A native dataset to 3.20 Å resolution was collected, and the obtained phases were extended using DM [23]. The structure was built in Coot [24] and refinement was performed using PHENIX [25], including four-fold NCS, simulated annealing and TLS B-factor refinement. Final statistics can be found in Table I.

***In vitro* deubiquitination assays**

Prior to assaying the deubiquitinase activity of A20, the protein was activated by incubation with 10 mM DTT at room temperature for 10 minutes. *In vitro* deubiquitination assays were performed with 1.5 μg A20, 2.5 μg K63- or K48-linked tetraubiquitin chains as substrate, in 30 μl DUB-buffer (50 mM Tris [pH7.6], 5 mM DTT) at 37 °C. 5 μl aliquots of the reaction were taken at the time-points indicated, and the reaction was stopped by addition of 5 μl 2xSDS-sample buffer. Samples were subjected to SDS PAGE analysis with subsequent silver staining using the BioRad Silver Stain Plus Kit with the manufacturers protocol.

Results and Discussion

Structure determination

In order to investigate structural aspects of A20-mediated deubiquitination, the OTU domain (residues 1-366) was cloned from human cDNA, expressed as a GST-fusion protein in bacteria and purified to homogeneity (Material and Methods). The protein crystallised readily in widely varying conditions from commercial screens, but unfortunately, the predominant trigonal crystal form was perfectly twinned, and such crystals were of no use for experimental phasing techniques. A second crystal form could be obtained in a non-twinned monoclinic setting and the structure was determined using the anomalous signal from incorporated seleno-methionine. Phases were obtained to 3.7 Å resolution and extended to 3.2 Å data (obtained from a native crystal, see Material and Methods). The structure was built and refined with final statistics shown in Table I.

Overall structure

The structure of the A20 OTU domain is wedge-shaped, with two almost flat large surfaces and a helical stalk projecting from one side of the molecule (Fig. 1A). The core domain resembles the deubiquitinase Otubain-2 (Fig. 1B, [20]), which is the only protein in the protein data bank with similarities to A20 (Z-score 6.5, RMSD 2.9 Å over 129 aligned residues) in a DALI search [26].

This catalytic core present in A20 consists of a five-stranded β-sheet (β1-β5), sandwiched between helix α3 on one side, and two parallel helices (α4 and α8) packing against the other side. Four more helices (α1, α5, α6 and α7) form a second, perpendicular half-circle around α4 and α8. These regions (coloured blue in Figure 1) are also found in Otubain-2, with several differences (Fig. 1B, [20]). Otubain-2 has a four-stranded β-sheet (β3 in A20 has no counterpart) and α1 and α2 in Otubain-2 are located similarly to α3 of A20 but pack against the β-sheet differently. Helices α3 and α10 in Otubain-2 are structurally equivalent to α4 and α8 in A20. An insertion between helices α3 and α7 in Otubain-2 (comprising α4, α5 and α6) is not present in A20, but structurally mimicked by the A20 α1-helix (cyan in Figure 1). The helical

insertion in Otubain-2 is also present in Otubain-1 and Otubain-like proteins, but missing in the remaining annotated OTU domains in ProSite (profile PS50802 [27]). Helix α5 of A20 is considerably shorter than its counterpart in Otubain-2 (α7), whereas α6 and α7 in A20 (α8, α9 in Otubain-2) are extended, and are connected by a flexible loop of 10 residues that is disordered in the crystal structure (indicated by grey dotted lines in Fig. 1A, 2A). A second loop between β2 and β3 is disordered in both A20 and Otubain-2; these disordered regions are likely to be involved in ubiquitin binding (see below).

Two structural features of A20 are not present in the structure of Otubain-2. First, a helical stalk region extends the OTU core (in shades of yellow in Fig. 1A). This stalk is formed by packing of helices α2 and α11. A third region contributing to the stalk is the very N-terminus (residues 1-10), which is partly disordered in the crystal structure (first residue visible is Pro7). The core between those three regions is of a hydrophobic nature, and termination of the protein at residue 353 (lacking the last two visible turns of the C-terminal α11 helix) results in insoluble protein (data not shown).

The second region only present in A20 is formed by 70 residues (264-337) connecting β-strand β5 with the C-terminal helix α11 (coloured purple in Fig. 1A). These residues form two layers of β-hairpin loops connected by helices α9/α10. The top hairpin loop (as in Fig. 1A) is shorter, and supported by the lower hairpin loop (β7/β8). In an unusual extended fashion, a gap of 50 Å is bridged from the tip of the lower hairpin loop (residue 320) to the beginning of the C-terminal α11 helix (residue 337), spanning the whole surface of the molecule. Although this region is highly conserved (Fig. 2A, C) the significance of this extension is not clear at present.

The A20 OTU domain contains conserved surfaces for proximal and distal ubiquitin binding sites.

The structural features of A20 were analysed for conserved surface residues to investigate potential ubiquitin binding sites. A sequence alignment with the A20 OTU domain from different species was generated (Fig. 2A) and mapped onto the surface of the protein (Fig. 2B, C). A20 shows strongly

conserved features around the catalytic site, and in regions that can be assumed to comprise the binding sites for the proximal and distal ubiquitin (Fig. 2B). The position of the oxyanion hole relative to the catalytic cysteine, and superposition with known deubiquitinase:ubiquitin complexes (see Fig. 3 and below) onto A20 allows prediction of the position of the distal ubiquitin. In A20, two loops (residues 152-160 and 212-228) in this distal binding site are disordered despite high sequence conservation, and hence surface analysis in this region is not meaningful. Interestingly, conservation analysis also provides insights into the proximal ubiquitin binding site. The invariant residues Leu10, Asn98, Asp100, Thr118, and Gln187 are positioned to contact a proximal ubiquitin. However, to understand all features of the A20 OTU domain interactions with ubiquitin, protein complexes will be required.

Further examination of conserved residues surprisingly shows that the surface opposite of the active site is also highly conserved (Fig. 2C). This surface is mainly formed by the linker region between β8 and α11 (residues 330-340) and loop 263-271, which contribute numerous invariant residues (Glu332, Asn334, Arg271, Lys264, Ser266) to this surface. This surface region of the molecule is unlikely to contribute to ubiquitin binding, but might be involved in other protein-protein interactions, or in interactions with the C-terminal ZnF domains. Overall, several conserved surface patches in A20 can be derived from this analysis, and it will be interesting to see how and whether these contribute to A20 function.

Catalytic site environment

Cys proteases share a mechanistically common active site, which contains a catalytic triad consisting of the catalytic Cys (Cys103 in A20), a His residue to abstract the Cys proton and stabilize the nucleophile (His256 in A20), and a residue to stabilize the His residue (often negatively charged, potentially Asp70 in A20) (Fig. 3A). A second feature is an oxyanion hole close to the catalytic cysteine to stabilise the reaction intermediate. These features are conserved in Cys-dependent deubiquitinases of the USP, UCH and OTU families [28, 29]. Although these three protein families have entirely different folds, superposition aligns the active site remarkably well (Fig. 3). For the USP and UCH families, complex structures with ubiquitin suicide

substrates are available (HAUSP:Ub complex, 1nbf, [30], Fig. 3C; UCH-L1:Ub, 1xd3, [31], Fig. 3D), illuminating the position of the C-terminal residues of a distal ubiquitin at the catalytic site, and indicating the overall position of the ubiquitin molecule. In USP and UCH families, a Gln or Asn residue N-terminus of the catalytic Cys residue forms the oxyanion hole.

As mentioned above, A20 and Otubain-2 display several differences in structure, but share a conserved core domain harbouring the catalytic residues, which varies from the UCH/USP architecture (Fig. 3). While the catalytic Cys and His residues are structurally conserved, the third residue in the catalytic triad is different. In Otubain-2, two residues (Asn226 and Thr45) stabilize the His224 residue (Fig. 3B). The loop preceding the catalytic Cys51 in Otubain-2 is structurally in a different position from any other deubiquitinase, allowing Thr45 to maintain hydrogen bonds to His224 with sidechain and backbone atoms. Strikingly, this different loop also changes the oxyanion hole architecture, which is formed entirely by backbone amide groups from this loop [20].

A20 displays the same catalytic loop organisation as Otubain-2, and the catalytic residues Cys103 and His256 are structurally conserved, as is the oxyanion-loop (Fig. 3A, B). However, stabilisation of His256 for catalysis seems to be different in A20 compared to Otubain-2. In A20, similar backbone interactions with Thr97 are formed, however this residue is not conserved throughout species (Fig. 2A) and hence the side chain interaction might not be required for stabilisation. Furthermore, there is no Asn226-equivalent residue in A20; the residue in this position (Val258) is unable to stabilise the catalytic His256. Instead, a negatively charged residue, Asp70, is located in close proximity to His256. This residue does not form other electrostatic contacts, and although its distance from His256 is too far for a hydrogen bond (4.4 Å), minor rearrangement would suffice to allow this interaction. Furthermore, this residue is fully conserved (Fig. 2A). Asp70 is located on helix α3 that has no structural equivalent in Otubain-2.

43 out of 55 annotated OTU domains in Prosite (profile PS50802) contain an Asp/Asn/Glu residue two positions C-terminal to the catalytic His residue, mimicking the His224-Asn226 stabilisation seen in Otubain-2. The remaining 12 proteins contain residues incapable of His stabilisation such as

Val258 of A20. Comparison of sequences N-terminal to the catalytic cysteine in these proteins reveals that 10 out of these 12 proteins contain a negatively charged Glu or Asp residue at a position equivalent to Asp70 (the remaining two proteins are bacterial and viral OTU domain containing proteins with poor sequence similarity). These proteins are Cezanne-1 and 2, TRABID/ZRANB1 and VCIP135. Cezanne and TRABID are known interactors of TRAF proteins and may function similarly to A20 [32], while VCIP135 interacts with the ubiquitin dependent chaperone VCP/p97/cdc48 and plays roles in Golgi-formation after mitosis [33]. It is hence a possibility that the catalytic triad found in A20 is also present in Cezanne, TRABID and VCIP135.

In vitro deubiquitination activity

The A20 OTU domain has catalytic activity as a deubiquitinating enzyme, as it specifically cleaves isopeptide bonds formed between the C-terminal Gly76 carboxyl group of ubiquitin and the Nε amino-group of a substrate Lys residue. Isopeptide bonds link ubiquitin monomers, and as the seven different Lys residues on ubiquitin are located spatially in different places, ubiquitin chain structures differ radically depending on the ubiquitin lysine employed for chain formation. We tested the ability of the isolated A20 OTU domain to hydrolyse Lys63- and Lys48-linked tetraubiquitin chains *in vitro*. Interestingly, we found that the purified A20 OTU domain was able to hydrolyse Lys48-linked ubiquitin tetramers with higher activity compared to Lys63-linked tetraubiquitin (Fig. 4A).

The A20 OTU domain structure revealed the identity of the catalytic triad residues, indicating that Asp70 might serve in positioning and charging of the His residue in the catalytic triad. Using site-directed mutagenesis, the catalytic triad residues were mutated individually to Ala in residues 1 to 366 of A20 ($A20^{1-366}$), and the ability of the mutants to cleave Lys48-linked tetraubiquitin was tested, and compared to wild-type $A20^{1-366}$. While $A20^{C103A}$ and $A20^{H256A}$ are devoid of catalytic activity against K48-linked tetraubiquitin, reduced activity is seen in $A20^{D70A}$ (Fig. 4B). Residual activity of $A20^{D70A}$ is not surprising as the backbone interaction of His256 with Thr97 may also contribute to stabilising the imidazolium ion.

A20 contains seven A20 ZnF domains within its C-terminus, and recent work has shown that these domains have the ability to bind ubiquitin [13, 14], and might therefore serve as ubiquitin chain receptors and contribute to specificity of A20. We therefore tested whether longer versions of A20, including the first (A20 $^{1-413}$), the first two (A20 $^{1-505}$), three (A20 $^{1-565}$), and four (A20 $^{1-635}$) ZnF domains showed different ability to cleave Lys63-linked tetraubiquitin. All proteins showed similar activity towards Lys48-linked tetraubiquitin, and none cleaved Lys63-linked tetraubiquitin with increased activity compared to A20 $^{1-366}$ (data not shown). Hence we conclude that A20 gains its activity towards Lys63-polyubiquitin modified substrates in a different way, and is, unlike the second deubiquitinase in the NF-κB pathway, CYLD, not intrinsically endowed with bona-fide specificity for Lys63-linked polyubiquitin (Komander *et al.,* manuscript in preparation). One possible mechanism could be that A20 utilises interacting proteins as 'specificity factors'. ABIN family proteins contain a NEMO-like ubiquitin binding domain and bind to Lys63-linked ubiquitin chains (data not shown). ABINs interact with the C-terminal ZnF domains of A20 and might serve to co-localise A20 with Lys63-modified substrates. Further structural studies of full-length A20 and complexes with interacting proteins as well as ubiquitin chains will be required to shed light on the specificity determinants of A20.

Conclusions

We provide insights into the structure and catalytic mechanism of the deubiquitinase A20. This second structure of an OTU domain highlights the variability of the cysteine-protease fold. A20 lacks three helices only present in Otubain family members, and shows a characteristic C-terminal extension with two β-hairpins and a C-terminal α-helix. Further OTU domain structures will be required to understand the contribution of such regions to the OTU domain fold. A second interesting insight is the identification of Asp70 as an imidazolium ion stabilising residue in A20, which might have identified a subset of OTU domains which similar catalytic architecture. It will be important to obtain an (A20) OTU domain structure in complex with ubiquitin. Active site rearrangements, common in deubiquitinases upon substrate binding, are also

to be expected for A20; especially movement of helix α3 would be necessary to bring Asp70 closer to His256, and several disordered loops might become structured in the presence of ubiquitin. Finally our biochemical data show an *in vitro* preference of the A20 OTU domain for Lys48-linked polyubiquitin. This activity would directly antagonize a ligase activity conferred by the A20 C-terminus; hence modulation of the deubiquitinase activity towards Lys63-modified substrates *in vivo* seems necessary. Further characterisation of A20 interactions and regulation is likely to provide important insight into the cellular role of A20, and the signalling pathways leading to NF-κB activation.

Acknowledgments

DK is supported by a Beit Memorial Fellowship for Medical Research. This work was funded by Cancer Research UK.

The structure has been deposited with the protein data bank, with accession number XXXX.

Abbreviations: OTU, Ovarian Tumour; TNFα, tumour necrosis factor-α; NF-κB, nuclear factor κB; IκB, Inhibitor of NF-κB; IKK, IκB kinase; TAK1, TGFβ-activated kinase-1; TAB2, TAK1 binding protein-2; ABIN, A20 binding inhibitor of NF-κB; RIP1, Receptor-interacting protein-1; TRABID, TRAF binding domain; ZnF, A20-like zinc fingers; USP, Ubiquitin specific protease; UCH ubiquitin C-terminal hydrolase; VCIP135, VCP(p97)/p47 complex–interacting protein of 135 kD; UIM, ubiquitin interacting motif.

References

1 Hayden, M. S. and Ghosh, S. (2004) Signaling to NF-kappaB. Genes & development. **18**, 2195-2224

2 Perkins, N. D. (2007) Integrating cell-signalling pathways with NF-kappaB and IKK function. Nature reviews. **8**, 49-62

3 Opipari, A., Boguski, M. and Dixit, V. (1990) The A20 cDNA induced by tumor necrosis factor alpha encodes a novel type of zinc finger protein. J Biol Chem. **265**, 14705-14708

4 Beyaert, R., Heyninck, K. and Van Huffel, S. (2000) A20 and A20-binding proteins as cellular inhibitors of nuclear factor-kappa B-dependent gene expression and apoptosis. Biochemical pharmacology. **60**, 1143-1151

5 Heyninck, K. and Beyaert, R. (2005) A20 inhibits NF-kappaB activation by dual ubiquitin-editing functions. Trends Biochem Sci. **30**, 1-4

6 Lee, E., Boone, D., Chai, S., Libby, S., Chien, M., Lodolce, J. and Ma, A. (2000) Failure to regulate TNF-induced NF-kappaB and cell death responses in A20-deficient mice. Science. **289**, 2350-2354

7 Boone, D., Turer, E., Lee, E., Ahmad, R., Wheeler, M., Tsui, C., Hurley, P., Chien, M., Chai, S., Hitotsumatsu, O., McNally, E., Pickart, C. and Ma, A. (2004) The ubiquitin-modifying enzyme A20 is required for termination of Toll-like receptor responses. Nat Immunol. **5**, 1052-1060

8 Wertz, I., O'Rourke, K., Zhou, H., Eby, M., Aravind, L., Seshagiri, S., Wu, P., Wiesmann, C., Baker, R., Boone, D., Ma, A., Koonin, E. and Dixit, V. (2004) De-ubiquitination and ubiquitin ligase domains of A20 downregulate NF-kappaB signalling. Nature. **430**, 694-699

9 Adhikari, A., Xu, M. and Chen, Z. J. (2007) Ubiquitin-mediated activation of TAK1 and IKK. Oncogene. **26**, 3214-3226

10 Chen, Z. J. (2005) Ubiquitin signalling in the NF-kappaB pathway. Nat Cell Biol. **7**, 758-765

11 Evans, P. (2005) Regulation of pro-inflammatory signalling networks by ubiquitin: identification of novel targets for anti-inflammatory drugs. Expert reviews in molecular medicine. **7**, 1-19

12 Kovalenko, A. and Wallach, D. (2006) If the prophet does not come to the mountain: dynamics of signaling complexes in NF-kappaB activation. Mol Cell. **22**, 433-436

13 Lee, S., Tsai, Y., Mattera, R., Smith, W., Kostelansky, M., Weissman, A., Bonifacino, J. and Hurley, J. (2006) Structural basis for ubiquitin recognition and autoubiquitination by Rabex-5. Nat Struct Mol Biol. **13**, 264-271

14 Penengo, L., Mapelli, M., Murachelli, A., Confalonieri, S., Magri, L., Musacchio, A., Di Fiore, P., Polo, S. and Schneider, T. (2006) Crystal structure of the ubiquitin binding domains of rabex-5 reveals two modes of interaction with ubiquitin. Cell. **124**, 1183-1195

15 De Valck, D., Heyninck, K., Van Criekinge, W., Contreras, R., Beyaert, R. and Fiers, W. (1996) A20, an inhibitor of cell death, self-associates by its zinc finger domain. FEBS Lett. **384**, 61-64

16 Van Huffel, S., Delaei, F., Heyninck, K., De Valck, D. and Beyaert, R. (2001) Identification of a novel A20-binding inhibitor of nuclear factor-kappa B activation termed ABIN-2. J Biol Chem. **276**, 30216-30223

17 De Valck, D., Jin, D. Y., Heyninck, K., Van de Craen, M., Contreras, R., Fiers, W., Jeang, K. T. and Beyaert, R. (1999) The zinc finger protein A20 interacts with a novel anti-apoptotic protein which is cleaved by specific caspases. Oncogene. **18**, 4182-4190

18 Evans, P., Ovaa, H., Hamon, M., Kilshaw, P., Hamm, S., Bauer, S., Ploegh, H. and Smith, T. (2004) Zinc-finger protein A20, a regulator of inflammation and cell survival, has de-ubiquitinating activity. Biochem J. **378**, 727-734

19 Evans, P., Smith, T., Lai, M., Williams, M., Burke, D., Heyninck, K., Kreike, M., Beyaert, R., Blundell, T. and Kilshaw, P. (2003) A novel type of deubiquitinating enzyme. J Biol Chem. **278**, 23180-23186

20 Nanao, M., Tcherniuk, S., Chroboczek, J., Dideberg, O., Dessen, A. and Balakirev, M. (2004) Crystal structure of human otubain 2. EMBO Rep. **5**, 783-788

21 Pape, T. and Schneider, T. R. (2004) Hkl2map: a graphical user interface for macromolecular phasing with shelx programs. J Appl Cryst. **37**, 843-844

22 Bricogne, G., Vonrhein, C., Flensburg, C., Schiltz, M. and Paciorek, W. (2003) Generation, representation and flow of phase information in structure

determination: recent developments in and around SHARP 2.0. Acta Crystallogr D Biol Crystallogr. **59**, 2023-2030

23 Cowtan, K. and Main, P. (1998) Miscellaneous algorithms for density modification. Acta Crystallogr D Biol Crystallogr. **54**, 487-493

24 Emsley, P. and Cowtan, K. (2004) Coot: model-building tools for molecular graphics. Acta Crystallogr D Biol Crystallogr. **60**, 2126-2132

25 Adams, P. D., Grosse-Kunstleve, R. W., Hung, L. W., Ioerger, T. R., McCoy, A. J., Moriarty, N. W., Read, R. J., Sacchettini, J. C., Sauter, N. K. and Terwilliger, T. C. (2002) PHENIX: building new software for automated crystallographic structure determination. Acta Crystallogr D Biol Crystallogr. **58**, 1948-1954

26 Holm, L. and Sander, C. (1993) Protein structure comparison by alignment of distance matrices. J Mol Biol. **233**, 123-138

27 Hulo, N., Bairoch, A., Bulliard, V., Cerutti, L., De Castro, E., Langendijk-Genevaux, P. S., Pagni, M. and Sigrist, C. J. (2006) The PROSITE database. Nucleic acids research. **34**, D227-230

28 Amerik, A. Y. and Hochstrasser, M. (2004) Mechanism and function of deubiquitinating enzymes. Biochim Biophys Acta. **1695**, 189-207

29 Nijman, S. M., Luna-Vargas, M. P., Velds, A., Brummelkamp, T. R., Dirac, A. M., Sixma, T. K. and Bernards, R. (2005) A genomic and functional inventory of deubiquitinating enzymes. Cell. **123**, 773-786

30 Hu, M., Li, P., Li, M., Li, W., Yao, T., Wu, J. W., Gu, W., Cohen, R. E. and Shi, Y. (2002) Crystal structure of a UBP-family deubiquitinating enzyme in isolation and in complex with ubiquitin aldehyde. Cell. **111**, 1041-1054

31 Johnston, S. C., Riddle, S. M., Cohen, R. E. and Hill, C. P. (1999) Structural basis for the specificity of ubiquitin C-terminal hydrolases. Embo J. **18**, 3877-3887

32 Evans, P. C., Taylor, E. R., Coadwell, J., Heyninck, K., Beyaert, R. and Kilshaw, P. J. (2001) Isolation and characterization of two novel A20-like proteins. Biochem J. **357**, 617-623

33 Wang, Y., Satoh, A., Warren, G. and Meyer, H. H. (2004) VCIP135 acts as a deubiquitinating enzyme during p97-p47-mediated reassembly of mitotic Golgi fragments. J Cell Biol. **164**, 973-978

Figure legends

Figure 1.

A) Structure of the A20 OTU domain. Colouring of different structure features is described in the main text, and secondary structure elements are labelled. The active site residues are shown in stick representation. B) Structure of Otubain-2, with labelled secondary structure elements according to pdb-entry 1tff [20]. C) Superposition of A20 (coloured as in A) and Otubain-2 (in grey).

Figure 2.

A) Sequence alignment of the A20 OTU domain from different species, indicating sequence conservation in blue. Secondary structure elements are indicated with boxes for α-helices, arrows for β-sheets, and coloured according to Fig. 1A. Residues indicated by arrows are the catalytic site (red) and oxyanion hole (green). Grey dotted lines indicate disordered residues. B) Surface representation of the A20 OTU domain, coloured according to conservation from green (fully conserved) to red (not conserved). The active site and putative ubiquitin binding sites are indicated. C) Surface conservation on the A20 surface opposite of the active site. Several highly conserved surfaces are present which are unlikely to contribute to ubiquitin binding.

Figure 3.

A) Structure of A20, and close-up view of the active site in stereo representation. Catalytic residues are shown as ball-and-stick models, and hydrogen bonds are indicated as grey dotted lines. Catalytic residues are labelled in black, while residues forming the oxyanion hole are labelled in red. The sidechains of the oxyanion hole generating residues have been omitted for clarity in A and B. B) Otubain-2 (1tff, [20]), superposed onto A20, shown as in A. C) Structure of UCH-L1 in complex with ubiquitin vinyl sulfone (1xd3, [31]). The ubiquitin molecule is drawn in yellow, with stick representation for the C-terminal Gly residues. The position of the C-terminal glycine within the active site is shown; extra atoms from the vinyl sulfone group have been

omitted for clarity. D) Structure of HAUSP in complex with ubiquitin aldehyde (1nbf, [30]), shown as in C.

Figure 4.

A) *In vitro* activity of the isolated A20 OTU domain against Lys48- and Lys63-linked ubiquitin tetramers in a time course experiment, resolved on a silver-stained denaturing gradient gel. The various ubiquitin chain products are labelled, and the A20 OTU domain is indicated. M: molecular weight marker. A20 does contain activity against K63-linked ubiquitin chains at later time points in the experiment. B) *In vitro* activity of catalytic site point mutants against Lys48-linked tetraubiquitin compared to wildtype A20 as in A. Cys103, His256 and Asp70 are required for full catalytic activity.

Table I

Data collection and refinement statistics. Values between brackets are for the highest resolution shell. All measured data were included in structure refinement.

	A20 SeMet	A20 SeMet	A20 SeMet	A20 native
Data collection statistics	Peak	Inflection	Remote	
Beamline	ID29	ID29	ID29	ID14-2
Wavelength (Å)	0.97938	0.97948	0.97372	0.9340
Space Group	$P2_1$	$P2_1$	$P2_1$	$P2_1$
Unit Cell (Å)	*a* = 85.29 *b* = 83.34 *c* = 165.40 β = 98.123	*a* = 85.50 *b* = 83.46 *c* = 165.87 β = 98.149	*a* = 85.25 *b* = 83.32 *c* = 165.55 β = 98.067	*a* = 84.96 *b* = 83.02 *c* = 164.94 β = 98.082
Resolution (Å)	84.5-3.70 (3.90-3.70)	84.5-3.70 (3.90-3.70)	71.1-3.70 (3.90-3.70)	50-3.20 (3.37-3.20)
Observed reflections	125481 (18297)	60929 (8690)	72464 (10625)	152339 (22338)
Unique reflections	24875 (3602)	23319 (3337)	23601 (3459)	36226 (5247)
Redundancy	5.0 (5.1)	2.5 (2.6)	3.1 (3.1)	4.2 (4.3)
Completeness (%)	100 (100)	93.3 (91.8)	95.7 (96.8)	96.0 (95.9)
R_{merge}	0.112 (0.455)	0.110 (0.567)	0.130 (0.497)	0.075 (0.559)
$\langle I/\sigma I \rangle$	13.3 (3.5)	7.9 (1.6)	11.2 (3.2)	15.9 (2.6)
Phasing statistics				
Anomalous completeness	99.8 (99.9)	75.4 (71.4)	89.5 (89.8)	
Anomalous multiplicity	2.6 (2.6)	1.5 (1.5)	1.6 (1.6)	
Phasing Power (anomalous)	0.914			
<FOM>	0.373			
$\langle FOM \rangle_{DM}$ to 3.2Å	0.595			
Refinement statistics				
Reflections in test set				3606
R_{cryst}				0.227
R_{free}				0.259
Number of atoms				10192
Wilson *B* ($Å^2$)				98.1
$\langle B \rangle$ ($Å^2$)				114.9
RMSD from ideal geometry				
Bond length (Å)				0.007
Bond angles (°)				1.047

Biochemical Journal Immediate Publication. Published on 26 Oct 2007 as manuscript BJ20071399

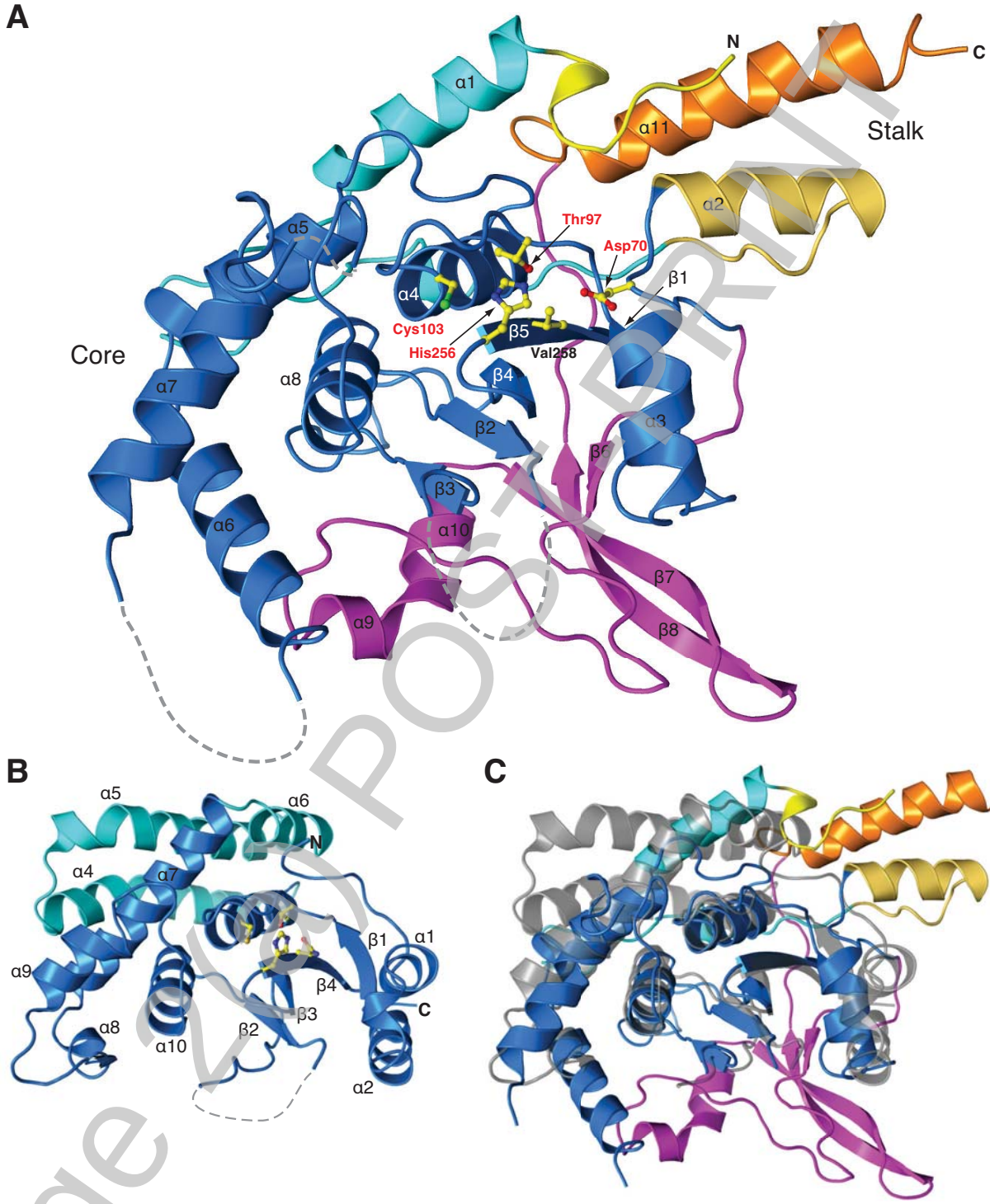

Figure 1

Biochemical Journal Immediate Publication. Published on 26 Oct 2007 as manuscript BJ20071399

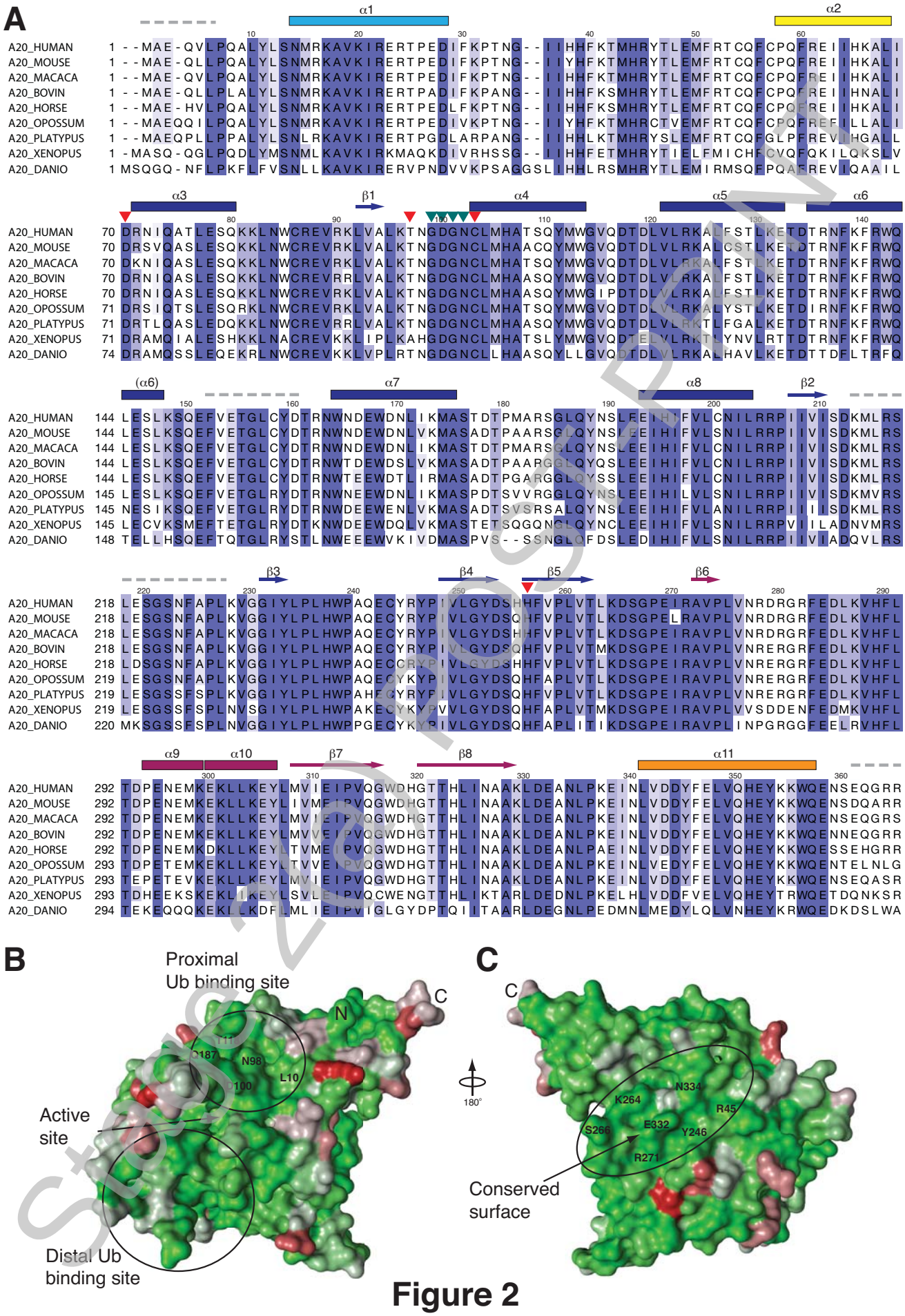

Figure 2

Biochemical Journal Immediate Publication. Published on 26 Oct 2007 as manuscript BJ20071399

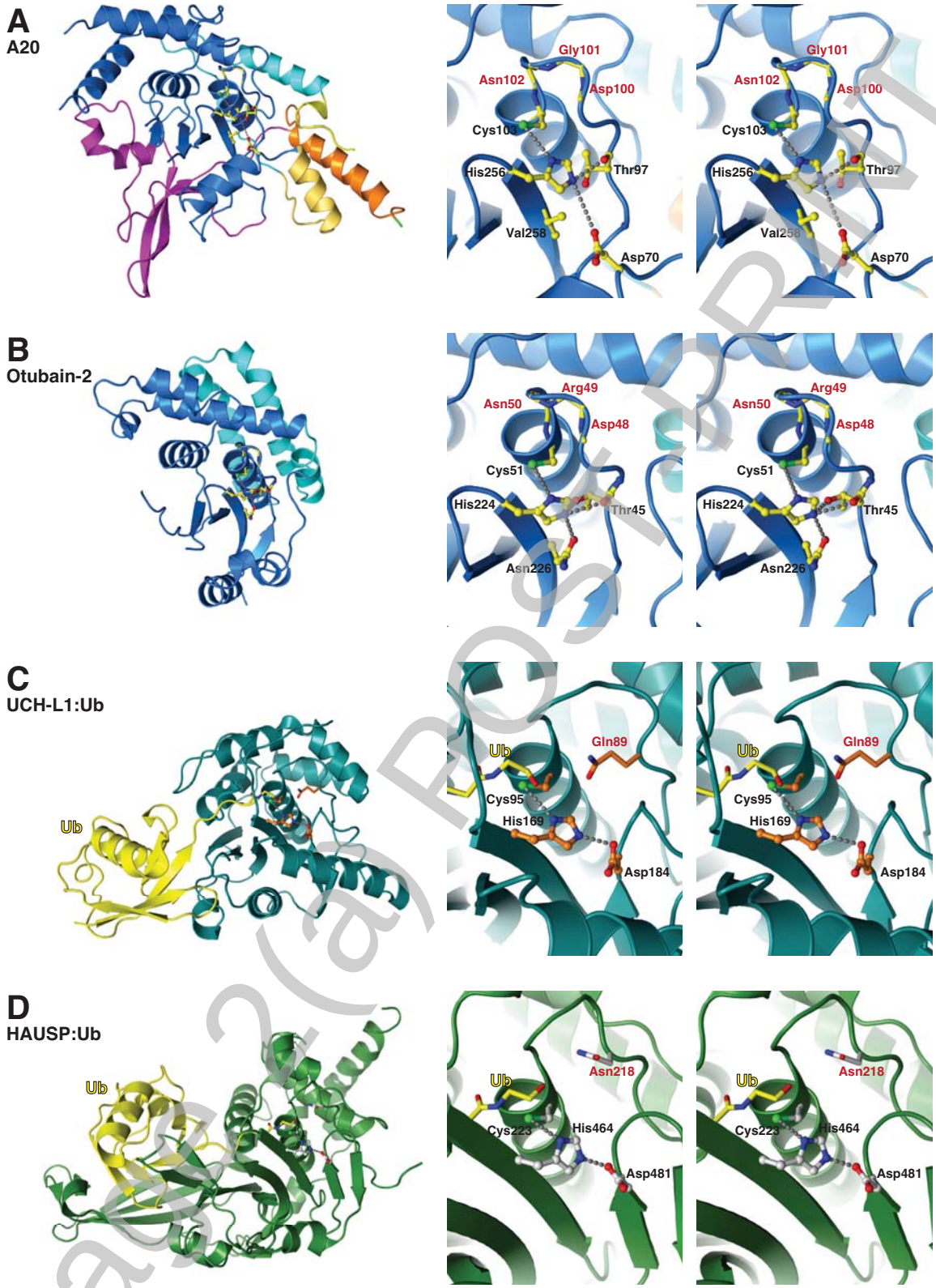

Figure 3

Biochemical Journal Immediate Publication. Published on 26 Oct 2007 as manuscript BJ20071399

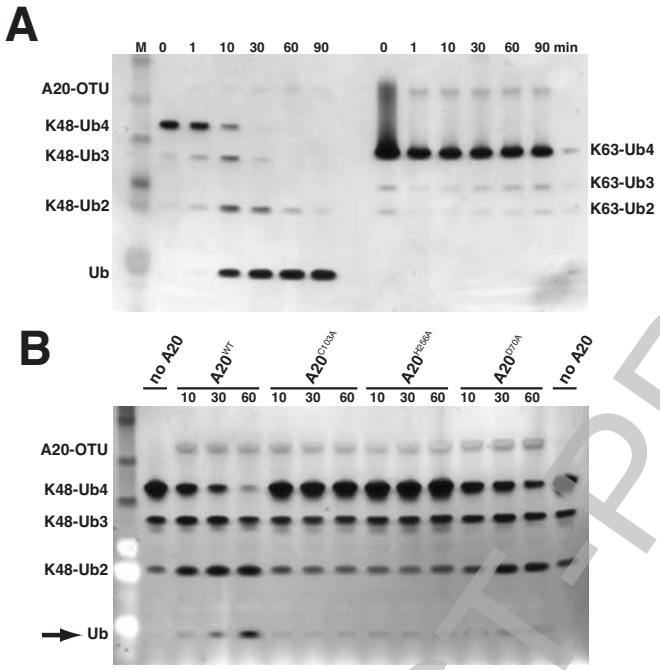

Figure 4